Physics of Plasmas ARTICLE scitation.org/journal/php

Suppression of power losses during laser pulse propagation in underdense plasma slab

Cite as: Phys. Plasmas **28**, 023112 (2021); doi: 10.1063/5.0036759
Submitted: 7 November 2020 · Accepted: 26 January 2021 ·
Published Online: 23 February 2021

View Online Export Citation CrossMark

K. V. Lezhnin,[a)] K. Qu, and N. J. Fisch

AFFILIATIONS

Department of Astrophysical Sciences, Princeton University, Princeton, New Jersey 08544, USA

[a)]Author to whom correspondence should be addressed: klezhnin@princeton.edu

ABSTRACT

For current state-of-the-art terawatt lasers, the primary laser scattering mechanisms in plasma include forward Raman scattering (FRS), excitation of plasma waves, and the filamentation instability. Using 2D particle-in-cell (PIC) simulations, we demonstrate that FRS dominates in the regime with medium-to-low density plasma and non-relativistic laser fields. We numerically show that FRS can be suppressed using a two-color laser with frequency detuning exceeding the plasma frequency, $\Delta\omega > \omega_{pe}$, leading to a more efficient laser energy transmission. An optimal laser pulse energy redistribution ratio is predicted analytically and verified by PIC simulations.

I. INTRODUCTION

In recent years, high power laser technology has reached the level of petawatt scale with kilojoule laser pulse energy.[1] High power laser-matter interactions result in the generation of high energy beams of charged particles[2–4] and photons,[5,6] offering a broad range of possible particle/light sources with numerous applications.[7]

In applications of laser-matter interactions, it is vital to transmit peak laser power to the target without incurring substantial energy loss. For example, in some approaches to laser-ion acceleration, efficient propagation of high laser power in pre-plasma surrounding the overdense target may help to achieve higher acceleration efficiency.[8,9] Similarly, the generation of γ rays through laser-solid interactions[10–13] requires propagation at high laser intensity. In both applications, the unwanted laser scattering happens mainly due to forward Raman scattering (FRS)[14] and filamentation instabilities (FI).[15,16] Yet another application requiring laser transmission at high power is a plasma-based laser amplifier, working through either backward Raman scattering[17] or stimulated Brillouin scattering.[18] Along with other effects, both the FRS and FI can interfere with this transmission.[19]

Several methods were explored and have demonstrated success in avoiding these instabilities: introducing a second laser with a slight frequency shift of the order of plasma frequency,[20–22] separating the total laser power into multiple subcritical laser pulses with the controlled coalescence of these pulses,[23,24] and introducing spatial incoherence of the laser pulse in order to avoid the critical power for FI.[25] The frequency detuning approach, or, more specifically, a two-color laser, was applied in laser wakefield acceleration[26] and is proposed to be used for electron–positron plasma generation,[27] among other applications (see references in Ref. 26).

Here we focus on the method of frequency detuning, where two detuned copropagating laser pulses can suppress both FRS and relativistic filamentation. The ponderomotive potential of the laser beat drives a plasma density modulation which can either enhance or suppress the instabilities depending on the laser frequency detuning, $\Delta\omega$. Specifically, our fully relativistic, kinetic particle-in-cell (PIC) simulations demonstrate that, by using two pulses with detuning $\Delta\omega/\omega_{pe} > 1$, laser power is propagated more efficiently owing to suppression of both FRS and FI. We also show the optimal energy partition of the frequency components for the maximum pulse power transmission.

Our finding supplements the findings by Kalmykov *et al.*,[20–22] namely, that the two-color laser scheme with $\Delta\omega > \omega_{pe}$ can avoid catastrophic relativistic filamentation within a propagation distance of a few Rayleigh lengths. Although their main interest is the suppression of relativistic self-focusing, their numerical simulations exhibit tail erosion due to FRS and electromagnetic cascades. The tail refers to the less intense, off-peak, part of a laser beam. Here we point out that, for parameters of interest, the most significant power loss is in fact caused by the slow-moving Stokes sidebands which temporally separate from the main pulse. Filamentation only modulates the laser pulse envelope. Thus, demonstrating the ability to suppress FRS broadens the applicability of the two-color laser scheme in long-distance high-power electromagnetic power propagation.

The paper is organized as follows: In Sec. II, we review the basic theoretical concepts and distinguish the dominant power loss mechanism. In Sec. III, we describe the setup of the numerical simulations. In Sec. IV, we discuss the simulation results and interpret them using simple theoretical estimates. In Sec. V, we compare our findings to previous descriptions of the detuning effect and summarize our results.

II. THEORETICAL BACKGROUND

An intense laser pulse, propagating in homogeneous rarefied plasma, drives plasma electrons to near relativistic speeds, thereby increasing the electron mass and decreasing the plasma frequency. The intensity-dependent change of the refractive index focuses the laser pulse, leading to relativistic self-modulation. The growth rate of FI[15,16] is

$$\gamma_{\mathrm{FI,max}} T_0 = \frac{\pi}{4} a_0^2 \frac{\omega_{\mathrm{pe}}^2}{\omega_0^2} \frac{1}{(1+a_0^2)^{3/2}}, \tag{1}$$

where $\omega_0 = 2\pi/T_0$ is the laser frequency in vacuum, $T_0 = \lambda/c$ is the laser period, λ is the laser wavelength in vacuum, c is the speed of light in vacuum, and $\omega_{\mathrm{pe}} = (4\pi n_e e^2/m_e)^{1/2}$ is the plasma frequency of plasma with electron number density n_e. e and m_e denote the electric charge and mass of the electron, respectively. $a_0 = eE/m_e\omega_0 c = 0.85 \cdot \sqrt{I/10^{18}\,\mathrm{W/cm^2}} \cdot \lambda/1\,\mu\mathrm{m}$ is the dimensionless amplitude of the laser pulse. The FI growth rate is the same for longitudinal and transverse modes. However, the fastest growing modes of the instability depend on the direction of the mode, $k_{\mathrm{FI},\parallel}\lambda = \pi a_0$ for the mode parallel to the laser wave vector, and $k_{\mathrm{FI},\perp}\lambda = \pi a_0 \omega_{\mathrm{pe}}/\omega_0$ for the mode perpendicular to the laser wave vector. Another figure of merit to describe the growth of FI is the e-folding number $N_{\mathrm{e,FI}} = \gamma_{\mathrm{FI,max}} T_{\mathrm{int}}$ with T_{int} being the interaction time. For a finite width, a laser pulse with power greater than the critical power $P_{\mathrm{cr,rel}}$ would catastrophically focus itself on filaments. The commonly accepted critical power for the relativistic filamentation obtained both numerically and analytically[16] is

$$P_{\mathrm{cr,rel}} = 17\,\mathrm{GW} \cdot \frac{\omega_0^2}{\omega_{\mathrm{pe}}^2}. \tag{2}$$

For the current study, we ignore other sources of the filamentation, such as ponderomotive and thermal filamentation. The relativistic filamentation dominates for terawatt pulses on a few tens of picoseconds time scale[28] although these FI branches have smaller power thresholds.

Another major mechanism of power loss from the primary pulse is the development of FRS. It leads to the decay of the laser wave into plasma wave and a new electromagnetic wave with the wavevector

$$k_{\mathrm{FRS}} = \frac{\omega_0}{c} \sqrt{\left(1 - \frac{\omega_{\mathrm{pe}}}{\omega_0}\right)^2 - \frac{\omega_{\mathrm{pe}}^2}{\omega_0^2}}. \tag{3}$$

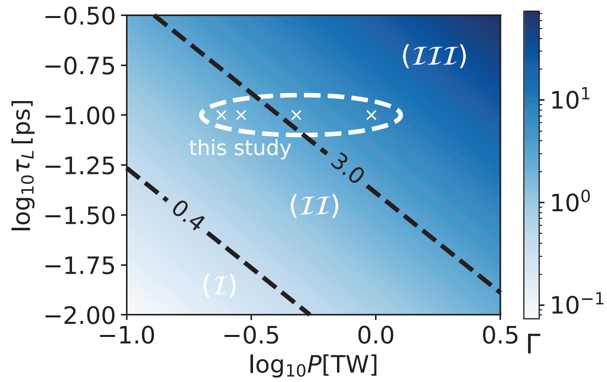

FIG. 1. Dependence of Γ on laser pulse power and duration for $n_e/n_{cr} = 0.05$ and $\lambda = 1\,\mu$m. The dashed black lines denote boundaries of regimes with $(\mathcal{I})$ FI domination, $(\mathcal{II})$ FI and FRS competing, and $(\mathcal{III})$ FRS domination. The white crosses demarcate our simulations parameters.

With sufficiently large amplitude and long interaction time, higher order FRS could appear at wavevectors $k_{\mathrm{FRS}}^{(p)}$ with order number p,

$$k_{\mathrm{FRS}}^{(p)} = \frac{\omega_0}{c} \sqrt{\left(1 - p \cdot \frac{\omega_{\mathrm{pe}}}{\omega_0}\right)^2 - \frac{\omega_{\mathrm{pe}}^2}{\omega_0^2}}. \tag{4}$$

Negative integer values of p will correspond to the anti-Stokes components of the FRS. The growth rate of the instability is[14]

$$\gamma_{\mathrm{FRS}} T_0 = \frac{\pi}{2} \frac{\omega_{\mathrm{pe}}^{3/2}}{\omega_0^{3/2}} \frac{a_0}{(1+a_0^2)^{7/4}}. \tag{5}$$

As we will show, this high-order FRS instability is observed in our simulations since the e-folding number $N_{\mathrm{e,FRS}} \equiv 2\gamma_{\mathrm{FRS}}(T_{\mathrm{int}}\tau_L)^{1/2}$ (Ref. 29) (τ_L is the laser pulse duration) exceeds 10 at the end of interaction.

While the straightforward comparison of the growth rates [Eqs. (1) and (5)] correctly captures the dominant instability at the early times of the interaction, the asymptotic integration of the laser envelope evolution equation is required to reproduce the physics at later stages of envelope evolution.[14] We categorize the laser parameters into different regimes by invoking the following criterion [see Eq. (71) from Ref. 14] based on the parameter

$$\Gamma \equiv \frac{P}{1\,\mathrm{TW}} \cdot \frac{\tau_L}{1\,\mathrm{ps}} \cdot \left(\frac{n_e}{10^{19}\,\mathrm{cm^{-3}}}\right)^{5/2} \cdot \left(\frac{\lambda}{1\,\mu\mathrm{m}}\right)^4. \tag{6}$$

FRS dominates if $\Gamma \geq 3$, and FI dominates if $\Gamma \leq 0.4$. We choose our simulation parameters to span over different interaction regimes where either FI and FRS compete or FRS dominates, as shown through the white crosses in Fig. 1. Thus, we expect the FRS to be the most dominant instability in our runs, while FI would be a secondary factor. Our simulations supplement those reported in Refs. 20–22 which solely focus on the FI-dominant regime.

III. SIMULATION SETUP

We perform 2D particle-in-cell (PIC) simulations using the code EPOCH.[30] We considered $\tau = 100$ fs Gaussian laser pulses with $w_0 = 20\,\mu$m waist and linear polarization (E_z is out of simulation plane $x-y$). The laser pulse dimensionless field a_0 ranges from 0.1 to 0.5 (peak intensities range from 6×10^{16} to 4×10^{17} W/cm^2) and the corresponding power $P/P_{cr,rel}=0.7-4.7$ covers the range of under/overcritical laser pulse powers. The uniform plasma locates between $x=5\,\mu$m and 3 mm, which is about 2.4 times the Rayleigh length $L_R=\pi w_0^2/\lambda$. The plasma is comprised of Maxwellian electrons with $T_e=10$ eV and immobile single-charged ions. The electron density is 5% of the critical density $n_{cr}=m_e\omega_0^2/4\pi e^2$. The simulation box dimension is $200\lambda\times100\lambda$ with the numerical resolution of 16 grid nodes per λ. Both longitudinal and transverse fastest FI modes fit in the box. Particles and electromagnetic fields are transmitted without reflection at the boundaries along both axes, unless mentioned specifically. The number of particles per cell is 10 per species. We use a moving window simulation setup, so the simulation window starts moving with the primary laser pulse group velocity $c\cdot\sqrt{1-n_e/n_{cr}}$ right after the laser pulse reaches the 2/3 of the simulation box. Moving at the laser group velocity, the simulation window fully captures the dynamics of the front of laser and plasma waves. The reduced window size allows us to simulate up to 10ps in order to track the evolution of the laser pulse envelope within the multiple e-folding times of FRS and FI instabilities.

To find out how the frequency detuning changes the propagation process, we perform a scan on the second laser pulse frequency. The corresponding laser pulse wavelength varies from 1 μm to 0.6 μm. In the case of these runs, we separate the total laser power equally into two pulses, one of them with $\lambda=1\,\mu$m, and another one with a smaller wavelength. Besides that, we scan the energy partition between two pulses with $\lambda=1\,\mu$m and 0.7 μm (frequency detuning $\Delta\omega/\omega_{pe}\approx1.91$) and three pulses with equally redistributed energy with $\lambda=1\,\mu$m, 0.75 μm, and 0.6 μm (corresponding to $\Delta\omega/\omega_{pe}\approx1.5$). We verify our results with the 32 nodes per micron grid resolution for a few runs with and without the frequency detuning. Auxiliary 1D and 2D simulations with periodic boundary conditions are also conducted in order to check the importance of the side scattering in the power propagation problem.

We measure the power losses in the process of the laser pulse propagation as the ratio of the electromagnetic energy left in the box to the initial energy of the laser pulse/pulses. Even though some energy of the laser pulse may be converted into other forms of the radiation (i.e., the energy is not actually dissipated, but propagates with group velocity slower/faster than moving window speed), we aim at the propagation of the significant peak power with the least amount of the pulse power lost in order to have an efficient further interaction. While this may not be required by all applications, laser ion acceleration above the 100 MeV threshold[31] and plasma-based laser amplification[32] will benefit from larger laser pulse powers delivered at the target surface.

IV. RESULTS

A. Single laser pulse propagation

First, let us discuss the simulation of the single undercritical laser pulse propagation in the underdense plasma. The considered run has $a_0\approx0.21$ (peak intensity $I=6\times10^{16}$ W/cm^2) and $n_e/n_{cr}=0.05$. The corresponding laser power $P/P_{cr,rel}\approx0.7$ and thus filamentation instability is not developed.

Figure 2(a) shows the electromagnetic energy density distribution of the laser pulse at $t=6$ ps, and Fig. 2(b) shows the transversely averaged longitudinal Fourier power spectrum of the electric field E_y at

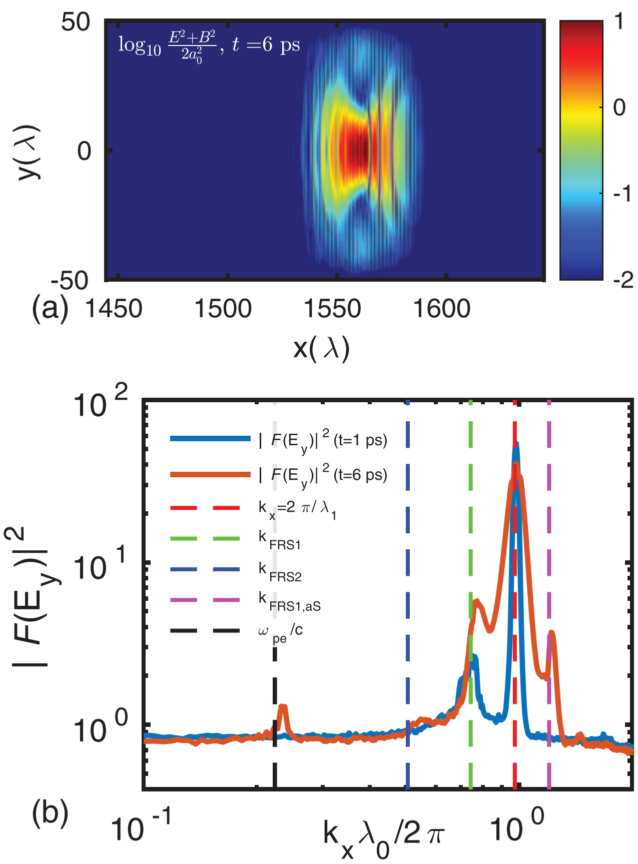

FIG. 2. (a) Normalized EM energy distribution and (b) Fourier power spectrum of the electric field E_y for $a_0=0.21$ and $n_e/n_{cr}=0.05$ at $t=1$ ps and 6 ps.

$t=1$ ps and 6 ps. We see both longitudinal and transverse modulations of the pulse envelope in Fig. 2(a). Both FI and FRS show their signatures in the Fourier power spectra shown in Fig. 2(b). Here, we present the longitudinal power spectrum of the laser pulse at the initial stage and after >10-e-folding growth of FRS instability (blue and brown line, respectively). Vertical lines represent various high-order FRS wavenumbers for the same parameters. The input laser pulse begins with a peak at $k_{med}=\omega_0/c\sqrt{1-\omega_{pe}^2/\omega_0^2}$. After $\sim$1 ps, the first-order FRS peak is developed near $k_{FRS,1}$. The second-order FRS peak is also shown as a small bump near $k_{FRS,2}$. Two other peaks are seen at the plasma wave wavenumber $k_{pe}=\omega_{pe}/c$ and anti-Stokes sideband $k_{FRS,-1}=\sqrt{(\omega_0+\omega_{pe})^2-\omega_{pe}^2}/c$. FRS peaks eventually grow to the order of the primary laser pulse peak height. The spectrum becomes flattened at the later stages, which may be attributed to longitudinal FI instability.[16] The resulting power loss after the interaction (at 10 ps) is 15% and is approximately the same for 1D and 2D simulations with periodic and outflow transverse boundary conditions.

To analyze the mechanisms of laser power loss, we show four snapshots of the laser pulse envelope and the plasma density, in Fig. 3. Figure 3(a) shows the initial laser pulse envelope at $t=1$ ps. At $t=6$ ps, FRS instability begins to modulate the laser pulse tail as shown in Fig. 3(b). The simulation time corresponds to $N_{e,FRS}\approx15$

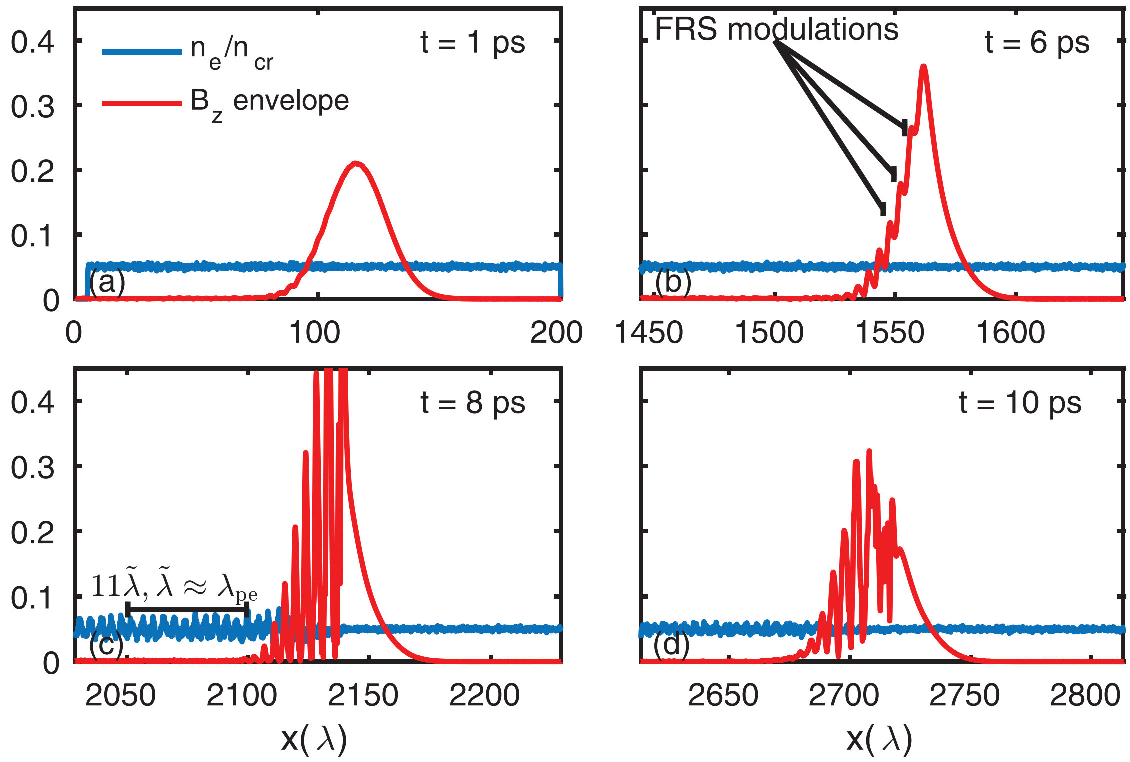

FIG. 3. Envelopes of the laser pulse B_z field in units of $m_e\omega_0 c/e$ (red curve) and plasma density (blue curve) with $P/P_{cr,rel} = 0.7$ at different times. (a) Initial stage, (b) development of FRS modulation, (c) separation of FRS photons and excitation of plasma waves with period $\tilde{\lambda} \approx \lambda_{pe}$, and (d) final state.

e-folding growth. The FRS sideband overlaps with the primary laser pulse, causing a 1.5 times larger amplitude. At $t = 8$ ps, Fig. 3(c) shows strong perturbation of the pulse envelope and periodic structure of the plasma density (blue line). The period of these structures is $\tilde{\lambda} \approx 4.35\lambda$, which is very close to $\lambda_{pe} = c/\omega_{pe} \approx 4.47\lambda$. Development of the plasma wave peak is also seen in the spectrum shown in Fig. 2(b). Since the Stokes FRS sidebands have smaller group velocities $v_{gr,FRS1} = c \cdot \sqrt{1 - n_e/n_{cr} \cdot \omega_0^2/\omega_{FRS}^2} \approx 0.83c$ than the primary laser pulse $v_{gr,1} = c \cdot \sqrt{1 - n_e/n_{cr}} \approx 0.97c$, they, together with the plasma wave, flow out from the left boundary of the simulation box and their energies are lost. For the simulation box length of 200 μm, they will be able to leave the moving window in ≈4.6 ps, as can be seen by comparing Figs. 3(b) and 3(d). A qualitatively similar behavior is observed for overcritical pulses as well although both FRS and FI happen much faster and lead to larger losses of power from the simulation box via FRS. It is also worth mentioning that even though we observe an excitation of the plasma waves in the wake of the laser pulse, the power, according to the Manley–Rowe relations,[33] is no more than $\omega_{pe}/\omega_{FRS} \approx 30\%$ in comparison to FRS photons.

B. Frequency detuning of the laser pulse into equal energy pulses

Next, we show how two copropagating laser pulses with a frequency detuning can suppress the power loss. We separate the total power into two laser pulses with a frequency detuning $\Delta\omega/\omega_{pe}$, following Refs. 20–22. In these works, it was shown that the frequency detuning $\Delta\omega/\omega_{pe} > 1$ helps to manipulate the pulse focusing effect, allowing for the more steady process of the laser pulse propagation by avoiding catastrophic self-focusing. While our figure of merit and laser-plasma parameters are different from ones in Refs. 20–22, it turned out that the same method can also suppress the FRS growth rates and corresponding power losses.

Figure 4 shows the evolution of the power spectrum for two-color laser pulse system with the total power $P/P_{cr,rel} \approx 0.7$ and the detuning $\Delta\omega/\omega_{pe} \approx 1.91$. In this case, the percentage of propagated energy is almost 100%. We see that there is only a slight broadening of spectrum peaks corresponding to $\lambda_1 = 1\,\mu$m and $\lambda_2 = 0.7\,\mu$m. FRS peaks do not develop significantly. Comparing with the spectrum of a single laser pulse with the same $P/P_{cr,rel}$ and n_e/n_{cr} in Fig. 2(b), the FRS peaks developed in the two-color scheme case are at least five times lower.

Finally, we show in Fig. 5 the fraction of transmitted energy and energy loss rate for different frequency detunings. The curves represent different total laser pulse powers $P/P_{cr,rel} \approx 0.7, 1.4, 2.35, 4.7$. The frequency detuning spans from $\Delta\omega/\omega_{pe} = 0$ to 3. The plasma density is $n_e/n_{cr} = 0.05$. The left panel shows the fraction of the injected energy propagated through the plasma slab of length L_x; the right panel shows the energy loss rate from the moving window. It clearly demonstrates the function of frequency detuning. For small detunings $\Delta\omega/\omega_{pe} < 1$, there is no significant suppression of power loss. For $|\Delta\omega/\omega_{pe} - 1| \ll 1$, FRS is resonantly driven to worsen the power propagation efficiency in comparison to a single pulse case. However, $\Delta\omega/\omega_{pe} > 1$ shows up to 50% efficiency increase in transmitted energy fraction.

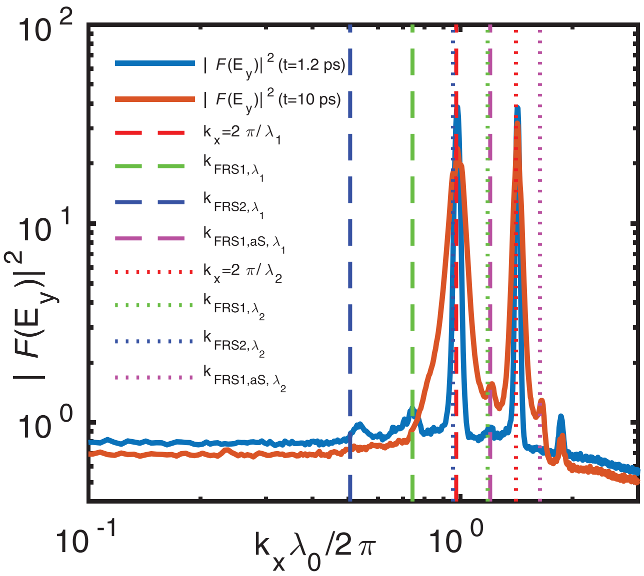

FIG. 4. Spectra of the two-color laser pulse before and after propagating through underdense plasma of length L_x with $n_e/n_{cr} = 0.05$ for $t = 10$ ps. The detuning is $\Delta\omega/\omega_{pe} \approx 1.91$.

C. Frequency detuning of the laser pulse into unequal energy pulses

The possible explanation may be formulated in terms of the FRS growth rates—recalling that $\gamma_{FRS} \propto \sqrt{I}\lambda^{3/2}$, we may argue that propagating power with shorter wavelength is more efficient since it allows to suppress FRS development. Even further suppression of the FRS may be achieved by separating the total energy (=total intensity) into pulses with different wavelengths. Auxiliary 1D simulations and 2D simulations with periodic transverse boundary conditions suggested that the side scattering, if present, is not a major contributor to the total power loss.

We perform a scan on energy ratio between two pulses, ranging from 0.01 to 100, including simulations with the whole energy in one of the wavelengths. Frequency detuning is chosen to be $\Delta\omega/\omega_{pe} = 1.9, 3, 4, 6$, respectively. Figure 6 summarizes the results of the scan. Figure 6(a) shows how the power transmission efficiency depends on energy ratio for $\Delta\omega/\omega_{pe} = 1.9$. The curves reveal that there is an optimal energy distribution ratio at which the power losses are minimized. Nontrivially, the optimal energy distribution ratio is not 1, but near $\sim$0.2.

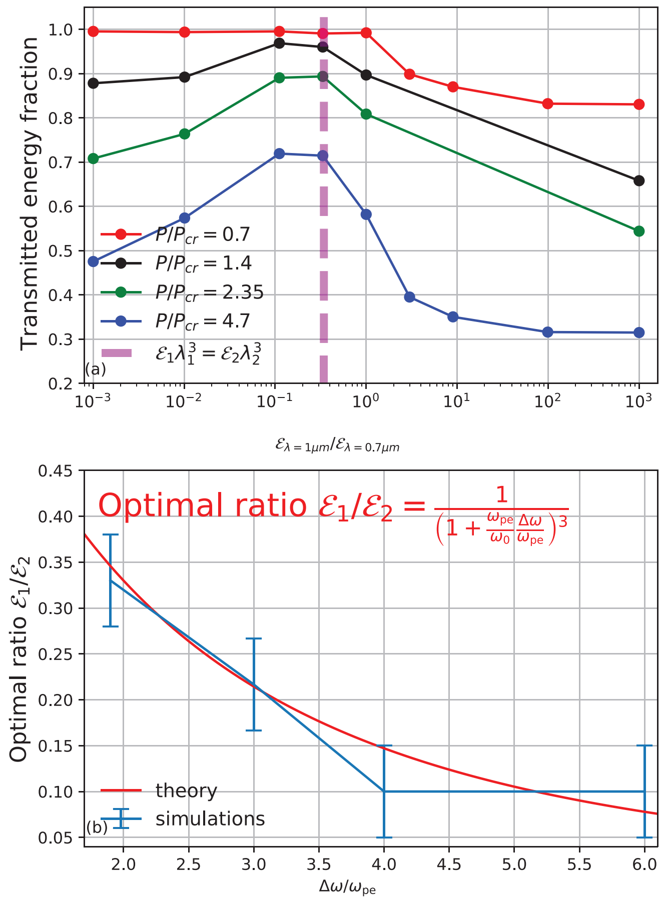

FIG. 6. (a) Transmitted energy vs energy partition ratio for simulations with $\Delta\omega/\omega_{pe} \approx 1.91$. The dashed magenta line demonstrates a theoretically predicted optimum. (b) Dependence of optimal laser energy ratio, x_{opt}, on frequency detuning $\Delta\omega/\omega_{pe}$.

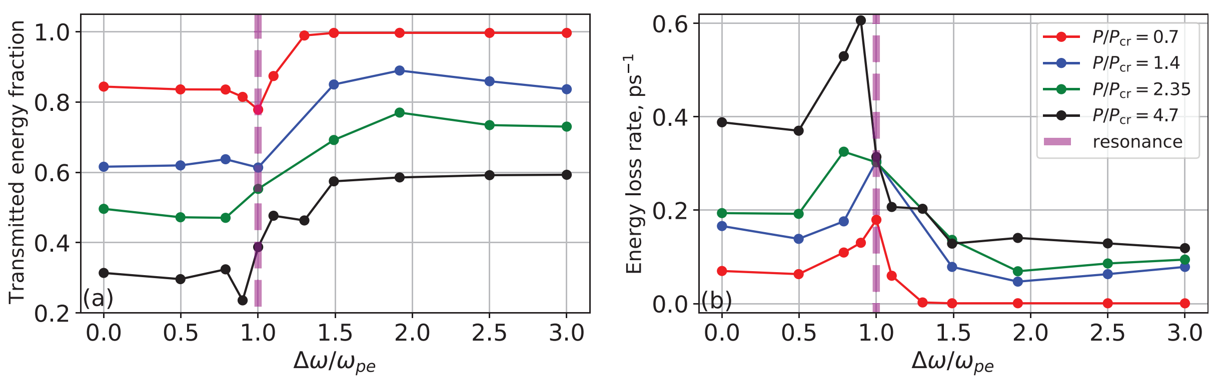

FIG. 5. (a) Transmitted energy vs frequency detuning $\Delta\omega/\omega_{pe}$; (b) peak energy loss rate vs $\Delta\omega/\omega_{pe}$ for equal energy laser pulses with $n_e/n_{cr} = 0.05$. For $\Delta\omega/\omega_{pe} > 1$, the power transmission is clearly more efficient as the power loss rate is significantly suppressed.

Since the dominating power loss factor is FRS, the nontrivial optimization of the energy distribution ratio for the maximum power transmission can be explained by analyzing the FRS growth rates. Assuming the two frequency components grow independently, the observed two-color laser FRS growth rate is the maximum growth rate of FRS for each wavelength (λ_1 and λ_2 are first and second laser pulse wavelengths, respectively; $\lambda_1 \geq \lambda_2$)

$$\gamma_{\rm FRS}^{2c} = \max\left(\gamma_{\rm FRS}^{\lambda_1}, \gamma_{\rm FRS}^{\lambda_2}\right). \tag{7}$$

We normalize it to the single-color laser FRS growth rate (corresponding to λ_1), $\gamma_{\rm FRS}^{1c}$, and define

$$\tilde{\gamma} \equiv \max\left(\frac{\gamma_{\rm FRS}^{\lambda_1}}{\gamma_{\rm FRS}^{0}}, \frac{\gamma_{\rm FRS}^{\lambda_2}}{\gamma_{\rm FRS}^{0}}\right) = \max\left(x^{1/2}, (1-x)^{1/2}\frac{\lambda_2^{3/2}}{\lambda_1^{3/2}}\right), \tag{8}$$

where $x = \mathcal{E}_1/\mathcal{E}_{tot}$ is the ratio of the energy of the first pulse to the total energy of the laser system. Figure 7 shows the dependence of the optimal two-color laser FRS growth rate $\tilde{\gamma}$ on x and frequency detuning $\Delta\omega/\omega_{\rm pe}$. It is seen that the optimal energy distribution starts from 0.5 at negligible detuning $\Delta\omega$ and decreases at larger $\Delta\omega$. Note that the analysis assumes independent FRS for the two frequency components. This assumption is violated at $\Delta\omega = \omega_{\rm pe}$ when the two components resonantly excite FRS. The minimum of $\tilde{\gamma}$ can be found by equalizing both terms in brackets in Eq. (8). It will lead to the optimization condition

$$\mathcal{E}_1\lambda_1^3 = \mathcal{E}_2\lambda_2^3. \tag{9}$$

The yellow line shows an optimal direction in $(x, \Delta\omega/\omega_{\rm pe})$ space. We plot the dashed magenta line in Fig. 6 to show the agreement with the numerical results. We repeat the numerical simulations with different detunnings varying from $\Delta\omega/\omega_{\rm pe} = 1.9$ to 6 and summarize the optimal ratio in Fig. 6(b). Note that the error bar width of 0.1 corresponds

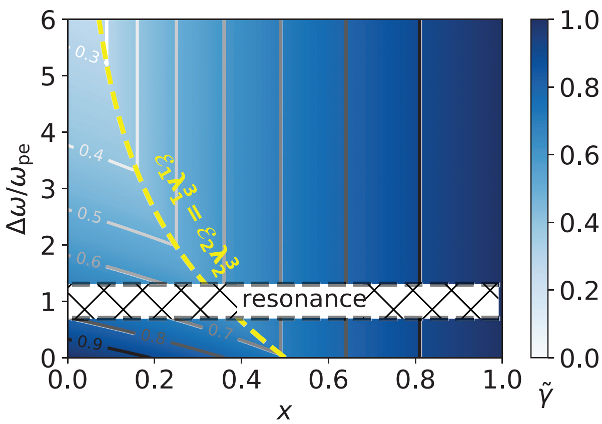

FIG. 7. Normalized two-color laser FRS growth rate, $\tilde{\gamma}$, as the function of energy partition ratio x and frequency detuning $\Delta\omega/\omega_{\rm pe}$. The hatched region corresponds to the FRS resonance $\Delta\omega/\omega_{\rm pe} \approx 1$, and hence it should be avoided. The yellow dashed line represents an optimal regime for the FRS suppression.

to the step in the energy ratio of the simulations. The result shows a decent agreement with optimization condition, Eq. (9).

In the similar fashion, it is possible to use more than two pulses for a more efficient power transfer. We performed a few preliminary runs with three pulses separated between each other by at least $\Delta\omega/\omega_{\rm pe} \approx 1.5$. We saw that using three pulses further increases the power transmission efficiency, in agreement with $\tilde{\gamma}$ scaling of $1/\sqrt{N_{\rm p}}$, where $N_{\rm p}$ is the number of pulses. The energy partition can be optimized among multiple pulses for the best efficiency. Generalization of the approach described here for $N_{\rm p} \gg 1$ and ultimately getting into the incoherent pulse regime is of interest as well,[34] but it will be addressed in the separate work.

V. SUMMARY AND DISCUSSION

In summary, we discussed how to optimally transmit laser power using a multi-color system through the cold uniform underdense plasma slab by avoiding FRS and FI. Using 2D PIC simulations, we identified the primary role of FRS in power losses. We further demonstrated how frequency detuning suppresses the FRS power losses. FI acts only as a secondary factor by modulating the pulse envelope, which leads to modifications in local FRS growth rates. We showed that the frequency detuning for the efficient power transmission should be $\Delta\omega/\omega_{\rm pe} > 1$, and the resonant regime with $\Delta\omega \approx \omega_{\rm pe}$ should be avoided. By considering the unequal energy partition between detuned pulses and varying the total number of pulses, we found that the frequency detuning has an optimal energy ratio between two pulses, thus verifying the importance of the pulse interplay for the efficient power transmission. Using more than two pulses further improves the transmission efficiency. The extension to multiple pulses suggests the use of an entirely incoherent laser pulse to even further increase the power transmission efficiency.[34]

Let us compare our results with the results from Kalmykov *et al.*,[20–22] where the frequency detuning approach was also used, but aimed at suppression of FI. Both our and their studies conclude that FRS and longitudinal FI play a dominant role at the later stages of pulse evolution after the pulse traveled for an extended distance $X > L_R$. It was claimed in Ref. 21 that the electromagnetic cascading (i.e., the development of higher order FRS modes) cannot be neglected starting from $X \approx 3L_R/8$ for $\Delta\omega/\omega_{\rm pe} \approx 2$ and equal energy partition case.[20] The corresponding Stokes FRS modes are indeed seen in our simulations at $t \approx 1$ ps (see Fig. 4). The laser energy depletion reported in Ref. 22 is in reasonable agreement with our simulations with $P/P_{\rm cr} = 0.7$, $\Delta\omega/\omega_{\rm pe} \approx 1.3$ and $P/P_{\rm cr} = 1.4$, $\Delta\omega/\omega_{\rm pe} \approx 1.5$. The overall higher laser energy depletion in our simulations apparently is due to higher $\omega_{\rm pe}/\omega_0$ value than in Ref. 22. The discrepancy in the most dominant instability at the initial stage of the laser-plasma interaction can be explained by invoking the criteria for the dominance of FRS and FI instabilities [Eq. (6)]: using parameters of simulations in Refs. 20–22 ($P = 55$ TW, $\tau_L = 1.3$ ps, $n_e = 5.65 \times 10^{17}$ cm^{-3}, $\lambda = 0.8\,\mu$m), we get that in their case, FI is dominant over FRS ($\Gamma \approx 0.022$), and for parameters of our simulations it is the opposite ($\Gamma \geq 1.8$).

It is worth noting how our results described above will transition to the realistic 3D case. FRS and its suppression primarily take place in the longitudinal direction. We conduct 2D simulations to verify that filamentation, i.e., transverse change of laser energy and plasma density, is indeed negligible with the parameters of our interest. This is shown by observing dominant laser energy loss opposite to the laser direction and negligible side-scattering. Since the critical power for filamentation does not change in a reduced dimension, our 2D simulations should correctly capture this threshold behavior. It is thought that 2D simulations underestimate filamentation growth rate[35,36] if the laser power is above the critical value. We have taken into account this caveat and confine our simulations and discussions in the FRS dominated region in which filamentation is theoretically negligible in all cases. Therefore, we expect that more resource-demanding 3D simulations should generate the same conclusions.

The results obtained in our work broaden the applicability of this scheme, highlighting the benefits of multi-color laser systems in terms of an efficient laser power transmission through medium-to-low underdense plasma.

ACKNOWLEDGMENTS

This work was supported by NNSA DENA0003871 and AFOSR FA9550–15-1–0391. The EPOCH code was developed as part of the UK EPSRC Funded Project No. EP/G054940/1. The simulations presented in this article were performed on computational resources managed and supported by Princeton Research Computing, a consortium of groups including the Princeton Institute for Computational Science and Engineering (PICSciE) and the Office of Information Technology's High Performance Computing Center and Visualization Laboratory at Princeton University.

DATA AVAILABILITY

The data that support the findings of this study are available from the corresponding author upon reasonable request.

REFERENCES

[1]A. V. Korzhimanov, A. A. Gonoskov, E. A. Khazanov, and A. M. Sergeev, Phys.-Usp. **54**, 9 (2011).
[2]T. Tajima and J. M. Dawson, Phys. Rev. Lett. **43**, 267 (1979).
[3]V. Malka, S. Fritzler, E. Lefebvre, M.-M. Aleonard, F. Burgy, J.-P. Chambaret, J.-F. Chemin, K. Krushelnick, G. Malka, S. P. D. Mangles, Z. Najmudin, M. Pittman, J.-P. Rousseau, J.-N. Scheurer, B. Walton, and A. E. Dangor, Science **22**, 1596 (2002).
[4]A. Macchi, M. Borghesi, and M. Passoni, Rev. Mod. Phys. **85**, 751 (2013).
[5]S. Kneip, C. McGuffey, J. L. Martins, S. F. Martins, C. Bellei, V. Chvykov, F. Dollar, R. Fonseca, C. Huntington, G. Kalintchenko, A. Maksimchuk, S. P. D. Mangles, T. Matsuoka, S. R. Nagel, C. A. J. Palmer, J. Schreiber, K. T. Phuoc, A. G. R. Thomas, V. Yanovsky, L. O. Silva, K. Krushelnick, and Z. Najmudin, Nat. Phys. **6**, 980 (2010).
[6]S. Cipiccia, M. R. Islam, B. Ersfeld, R. P. Shanks, E. Brunetti, G. Vieux, X. Yang, R. C. Issac, S. M. Wiggins, G. H. Welsh, M.-P. Anania, D. Maneuski, R. Montgomery, G. Smith, M. Hoek, D. J. Hamilton, N. R. C. Lemos, D. Symes, P. P. Rajeev, V. O. Shea, J. M. Dias, and D. A. Jaroszynski, Nat. Phys. **7**, 867 (2011); K. Ta Phuoc, S. Corde, C. Thaury, V. Malka, A. Tafzi, J. P. Goddet, R. C. Shah, S. Sebban, and A. Rousse, Nat. Photonics **6**, 308 (2012).
[7]H. Daido, M. Nishiuchi, and A. S. Pirozhkov, Rep. Prog. Phys. **75**, 056401 (2012).
[8]T. Zh. Esirkepov, J. K. Koga, A. Sunahara, T. Morita, M. Nishikino, K. Kageyama, H. Nagatomo, K. Nishihara, A. Sagisaka, H. Kotaki, T. Nakamura, Y. Fukuda, H. Okada, A. S. Pirozhkov, A. Yogo, M. Nishiuchi, H. Kiriyama, K. Kondo, M. Kando, and S. V. Bulanov, Nucl. Instrum. Methods Phys. Res., Sect. A **745**, 150 (2014).
[9]K. V. Lezhnin, F. F. Kamenets, T. Z. Esirkepov, S. V. Bulanov, O. Klimo, S. Weber, and G. Korn, Phys. Plasmas **23**, 053114 (2016).
[10]T. Nakamura, J. K. Koga, T. Zh. Esirkepov, M. Kando, G. Korn, and S. V. Bulanov, Phys. Rev. Lett. **108**, 195001 (2012).
[11]C. P. Ridgers, C. S. Brady, R. Duclous, J. G. Kirk, K. Bennett, T. D. Arber, A. P. L. Robinson, and A. R. Bell, Phys. Rev. Lett. **108**, 165006 (2012).
[12]K. V. Lezhnin, P. V. Sasorov, G. Korn, and S. V. Bulanov, Phys. Plasmas **25**, 123105 (2018).
[13]T. Wang, X. Ribeyre, Z. Gong, O. Jansen, E. d'Humières, D. Stutman, T. Toncian, and A. Arefiev, Phys. Rev. Appl. **13**, 054024 (2020).
[14]W. B. Mori, IEEE J. Quantum Electron. **33**, 1942 (1997).
[15]C. E. Max, J. Arons, and A. B. Langdon, Phys. Rev. Lett. **33**, 209 (1974).
[16]E. Esarey, P. Sprangle, J. Krall, and A. Ting, IEEE J. Quantum Electron. **33**, 1879 (1997).
[17]V. M. Malkin, G. Shvets, and N. J. Fisch, Phys. Rev. Lett. **82**, 4448 (1999).
[18]R. D. Milroy, C. E. Capjack, and C. R. James, Phys. Fluids **22**, 1922 (1979); A. A. Andreev, C. Riconda, V. T. Tikhonchuk, and S. Weber, Phys. Plasmas **13**, 053110 (2006); G. Lehmann and K. Spatschek, *ibid.* **20**, 073112 (2013); S. Weber, C. Riconda, L. Lancia, J.-R. Marquès, G. A. Mourou, and J. Fuchs, Phys. Rev. Lett. **111**, 055004 (2013); M. R. Edwards, Q. Jia, J. M. Mikhailova, and N. J. Fisch, Phys. Plasmas **23**, 083122 (2016).
[19]A. A. Solodov, V. M. Malkin, and N. J. Fisch, Phys. Plasmas **10**, 2540 (2003); R. M. G. M. Trines, F. Fiuza, R. Bingham, R. A. Fonseca, L. O. Silva, R. A. Cairns, and P. A. Norreys, Nat. Phys. **7**, 87 (2011); N. A. Yampolsky and N. J. Fisch, Phys. Plasmas **18**, 056711 (2011); V. M. Malkin and N. J. Fisch, Eur. Phys. J.: Spec. Top. **223**, 1157 (2014).
[20]S. Kalmykov and G. Shvets, Phys. Plasmas **13**, 056707 (2006).
[21]S. Kalmykov, S. A. Yi, and G. Shvets, Phys. Rev. E **78**, 057401 (2008).
[22]S. Kalmykov, S. A. Yi, and G. Shvets, Plasma Phys. Controlled Fusion **51**, 024011 (2009).
[23]G. A. Askar'yan, S. V. Bulanov, F. Pegoraro, and A. M. Pukhov, J. Exp. Theor. Phys. **60**(4), 240 (1994).
[24]S. R. Fairchild, W. Walasik, D. Kepler, M. Baudelet, N. M. Litchinitser, and R. Martin, Sci. Rep. **7**, 10147 (2017).
[25]V. M. Malkin and N. J. Fisch, Phys. Rev. Lett. **117**, 133901 (2016).
[26]S. Li, G. Li, Q. Ain, M. S. Hur, A. C. Ting, V. V. Kulagin, C. Kamperidis, and N. A. M. Hafz, Sci. Adv. **5**(11), eaav7940 (2019).
[27]Y.-Y. Chen, P.-L. He, R. Shaisultanov, K. Z. Hatsagortsyan, and C. H. Keitel, Phys. Rev. Lett. **123**, 174801 (2019).
[28]Z. Li, Y. Zuo, J. Su, and S. Yang, Phys. Plasmas **26**, 093102 (2019).
[29]E. Esarey, C. B. Schroeder, and W. P. Leemans, Rev. Mod. Phys. **81**, 1229 (2009).
[30]C. P. Ridgers, J. G. Kirk, R. Duclous, T. G. Blackburn, C. S. Brady, K. Bennett, T. D. Arber, and A. R. Bell, J. Comput. Phys. **260**, 273 (2014); T. D. Arber, K. Bennett, C. S. Brady, A. Lawrence-Douglas, M. G. Ramsay, N. J. Sircombe, P. Gillies, R. G. Evans, H. Schmitz, A. R. Bell, and C. P. Ridgers, Plasma Phys. Controlled Fusion **57**, 113001 (2015).
[31]A. Higginson, R. J. Gray, M. King, R. J. Dance, S. D. R. Williamson, N. M. H. Butler, R. Wilson, R. Capdessus, C. Armstrong, J. S. Green, S. J. Hawkes, P. Martin, W. Q. Wei, S. R. Mirfayzi, X. H. Yuan, S. Kar, M. Borghesi, R. J. Clarke, D. Neely, and P. McKenna, Nat. Commun. **9**, 724 (2018).
[32]V. M. Malkin and N. J. Fisch, Phys. Rev. E **101**, 023211 (2020).
[33]I. Y. Dodin, A. I. Zhmoginov, and N. J. Fisch, Phys. Lett. A **372**, 6094 (2008).
[34]M. R. Edwards, K. Qu, J. M. Mikhailova, and N. J. Fisch, Phys. Plasmas **24**, 103110 (2017).
[35]A. J. Schmitt, Phys. Fluids B **3**, 186 (1991).
[36]A. Pukhov and J. Meyer-ter-Vehn, Phys. Rev. Lett. **76**, 3975 (1996).